Human Molecular Genetics, 2008, Vol. 17, No. 19 **2921–2933**
doi:10.1093/hmg/ddn191
Advance Access published on July 11, 2008

The lamin B receptor under transcriptional control of C/EBPε is required for morphological but not functional maturation of neutrophils

Tatiana V. Cohen[1], Kimberly D. Klarmann[1,2], Krisada Sakchaisri[3], Jason P. Cooper[6], Douglas Kuhns[4], Miriam Anver[5], Peter F. Johnson[3], Simon C. Williams[6], Jonathan R. Keller[1,2] and Colin L. Stewart[1,*,†]

[1]Cancer and Developmental Biology Laboratory, CCR, [2]Basic Research Program, Laboratory of Cancer Prevention, SAIC-Frederick, Inc., [3]Laboratory of Protein Dynamics and Signaling, CCR, [4]Clinical Services Program, SAIC-Frederick, Inc. and [5]Laboratory Animal Sciences Program, Pathology/Histotechnology Laboratory, SAIC-Frederick, National Cancer Institute, Frederick, MD 21702, USA and [6]Department of Cell Biology and Biochemistry, Texas Tech University Health Sciences Center, Lubbock, TX 79430, USA

Received May 6, 2008; Revised and Accepted July 3, 2008

The lamin B receptor (LBR) is an integral nuclear envelope protein that interacts with chromatin and has homology to sterol reductases. Mutations in *LBR* result in Pelger–Huët anomaly and HEM–Greenberg skeletal dysplasia, whereas in mice *Lbr* mutations result in ichthyosis. To further understand the function of the LBR and its role in disease, we derived a novel mouse model with a gene-trap insertion into the *Lbr* locus (*Lbr*$^{GT/GT}$). Phenotypically, the *Lbr*$^{GT/GT}$ mice are similar to ichthyosis mice. The *Lbr*$^{GT/GT}$ granulocytes lack a mature segmented nucleus and have a block in late maturation. Despite these changes in nuclear morphology, the innate granulocyte immune function in the killing of *Staphylococcus aureus* bacteria appears to be intact. Granulocyte differentiation requires the transcription factor C/EBPε. We identified C/EBPε binding sites within the *Lbr* promoter and used EMSAs and luciferase assays to show that *Lbr* is transcriptionally regulated by C/EBPε. Our findings indicate that the *Lbr*$^{GT/GT}$ mice are a model for Pelger–Huët anomaly and that *Lbr*, under transcriptional regulation of C/EBPε, is necessary for morphological but not necessarily functional granulocyte maturation.

INTRODUCTION

Within the last decade, the functional architecture of the nucleus has undergone a fundamental re-evaluation, primarily due to a growing number of different diseases and anomalies (the nuclear envelopathies) are caused by mutations in proteins of the nuclear envelope (NE) and lamina (reviewed in 1). The NE is composed of an inner nuclear membrane (INM) and outer nuclear membrane, the latter being contiguous with the endoplasmic reticulum (ER). The NE and nuclear pore complexes that traverse the NE act as a selective barrier controlling the traffic of macromolecules, including proteins and RNAs, between the nucleus and the cytoplasm. Underlying the INM is the nuclear lamina, a thin proteinaceous layer that is primarily composed by the nuclear intermediate filament proteins, the A-type and B-type lamins. Besides maintaining the shape and mechanical strength of the interphase nucleus, the lamina has also been implicated in regulating DNA synthesis and chromatin organization (2).

The nuclear envelopathies are diseases resulting from mutations in the proteins associated with the NE and lamina (reviewed in 1). Most of these diseases are linked to mutations in the A-type lamin gene (*LMNA*) and are referred to as the laminopathies. The laminopathies result in skeletal muscle and cardiac defects, defects in adipocyte and bone

*To whom correspondence should be addressed. Tel: +1 6564070156; Fax: +1 6564642049; Email: colin.stewart@imb.a-star.edu.sg
†Present address: Institute of Medical Biology, 8A Biomedical Grove, Immunos, Singapore 138668, Singapore.

homeostasis, myelin degeneration and the premature aging diseases Hutchison–Gilford progeria and some cases of atypical Werner's syndrome (3).

In addition to the laminopathies, six other anomalies/diseases have been linked to mutations in NE-associated proteins (reviewed in 4). Among these proteins, the lamin B receptor (LBR) was initially discovered as a 58 kDa protein in turkey erythrocyte lysates that binds to lamin B, as well as lamin A with a lower affinity (5). LBR is an evolutionary conserved multifunctional integral membrane protein of the INM. The first third of the protein is hydrophilic and extends into the nucleoplasm. This domain interacts with chromatin in a cell cycle-dependent manner (6), Lamins B1/B2 (7), p34/p32—a putative splicing complex (8,9)—the chromatin binding protein HP1 (10), HA95—an RNA helicase A binding protein (11)—and p18, another integral membrane protein (12). During nuclear reassembly at mitosis, the LBR is important in targeting the NE to chromatin in an importin β-mediated process (13,14). The C-terminal third of LBR consists of eight transmembrane domains that exhibit sterol Δ-14-reductase activity under some conditions *in vitro* (15–17).

In humans, heterozygous mutations in the *LBR* gene result in the autosomal dominant Pelger–Huët anomaly (18) characterized by hypolobulation of granulocyte nuclei and altered chromatin structure. Homozygotes for a splicing anomaly in the *LBR* gene sometimes exhibit impaired cognitive development, heart defects and bone deformities (19–21). A homozygous LBR nonsense mutation resulted in a developmentally lethal metabolic disorder, HEM/Greenberg skeletal dysplasia, suggesting that LBR may be essential to proper cholesterol synthesis during development (22). However, this role of the LBR in developmental cholesterol regulation has recently been disputed (23). In mice, mutations in the *Lbr* gene result in ichthyosis (ic^J) of which the most overt phenotypes include alopecia, post-natal growth retardation, early lethality and syndactyly (18). Within the hematopoietic compartment of ic^J mice, splenic lymphocytes show clumping of heterochromatin. In the peripheral blood, neutrophils and eosinophils are immature and the nuclei are hypolobulated.

To further define the functional role of the LBR, we established a novel mouse line carrying a different mutation in the *Lbr* gene, specifically, a gene-trap insertion into the *Lbr* locus ($Lbr^{GT/GT}$). We compare this mutation to the ic^J mice and show that $Lbr^{GT/GT}$ homozygotes phenocopy ic^J mice, exhibiting embryonic lethality with incomplete penetrance, shortened post-natal lifespan, hydrocephaly and syndactyly, as well as chromatin atypia in the neutrophils. In addition, loss of LBR results in alterations to fibroblast nuclear morphology and the localization of other NE-associated proteins. We show that CCAAT/enhancer-binding protein epsilon (C/EBPε) transcriptionally regulates *Lbr* expression and that the *Lbr* is necessary for the morphological differentiation of granulocytes. Functional differentiation of granulocytes in their ability to kill bacteria did not appear to be impaired by the loss of LBR. Our data provide new evidence for the importance of the LBR in granulocyte development and reveal novel aspects to the significance of lamina/NEs in coordinating cellular functions.

RESULTS

Mapping the gene-trap insertion

To further determine the function of the LBR, we used an ES cell clone containing the gene-trap (pGT1Lxf) insertion into the *Lbr* locus (Supplementary Material, Fig. S1A). Southern and sequence analysis revealed the insertion of the gene-trap vector into exon 9 within the *Lbr* locus (Supplementary Material, Fig. S1B and E). The gene-trap plasmid pGT1Lxf contains an *en2* splice acceptor site and a β-galactosidase cDNA linked to the neomycin resistance cDNA (β-*geo*). Sequence analysis of genomic DNA showed that the cryptic splice donor site (SD1) within the vector resulted in splicing from exon 8 to the *En* splice acceptor within the vector (24). Cloning and sequencing the cDNA in the region of the insertion revealed that exon 9 is absent (Supplementary Material, Fig. S1E). Northern analysis of total RNA from heterozygous ($Lbr^{GT/+}$) fibroblasts revealed an additional 4.5 kb transcript containing *β-geo*, as well as the 3.4 kb wild-type transcript (Supplementary Material, Fig. S1C). The insertion predicts that 1199 bp of *Lbr* remains resulting in the translation of the first 366 of the 616 amino acid full-length protein. The gene-trapped *Lbr* allele produces a fusion protein consisting of the amino terminal nucleoplasmic domain and the first four transmembrane domains of LBR fused to β-geo and lacking the C-terminal sequences downstream of exon 8 (Supplementary Material, Fig. S1D). The fusion protein would have a predicted MW of 104 kDa. A polyclonal rabbit antibody to the LBR N-terminus detected a 58 kDa band corresponding to the endogenous LBR polypeptide in +/+ cells that was absent in $Lbr^{GT/GT}$ cells (Fig. 1G). However, due to the low expression of LBR in Primary Mouse Embryo Fibroblasts (PMEFs) some background bands were also observed in both wild-type and $Lbr^{GT/GT}$ cells. The larger fusion polypeptide was not detectable by immunoblotting using this antibody or an anti-lacZ antibody; however, we were able to visualize the expression of the fusion polypeptide using immunofluorescence in PMEFs. LBR is normally localized to the NE in wild-type cells (18) and, as shown in Supplementary Material, Figure S1F, the anti-LBR antibody detected a perinuclear staining pattern in wild-type PMEFs, which was not detected in gene-trapped PMEFs (upper panels). In contrast, an antibody to lacZ did not detect any specific staining pattern in wild-type PMEFs but revealed nuclear staining in gene-trapped PMEFs (lower panels), suggesting that the LBR–β-geo fusion protein is redistributed from the nuclear rim space to the nucleoplasm and cytoplasm.

$Lbr^{GT/GT}$ fibroblasts have nuclei with altered morphologies

To determine whether the loss of functional LBR from NE-affected nuclear morphology in $Lbr^{GT/GT}$ PMEFs, we analyzed the expression of chromatin and NE-associated proteins (Fig. 1). Immunostaining with antibodies to lamin B (Fig. 1A), lamin A/C and LAP2β (Fig. 1B) revealed that the lamina of $Lbr^{GT/GT}$ nuclei had a more wrinkled appearance compared with wild-type fibroblast nuclei. LBR also binds to heterochromatin protein 1 (HP1), a protein with diverse roles in chromatin organization and function (10). In wild-type cells, HP1α is

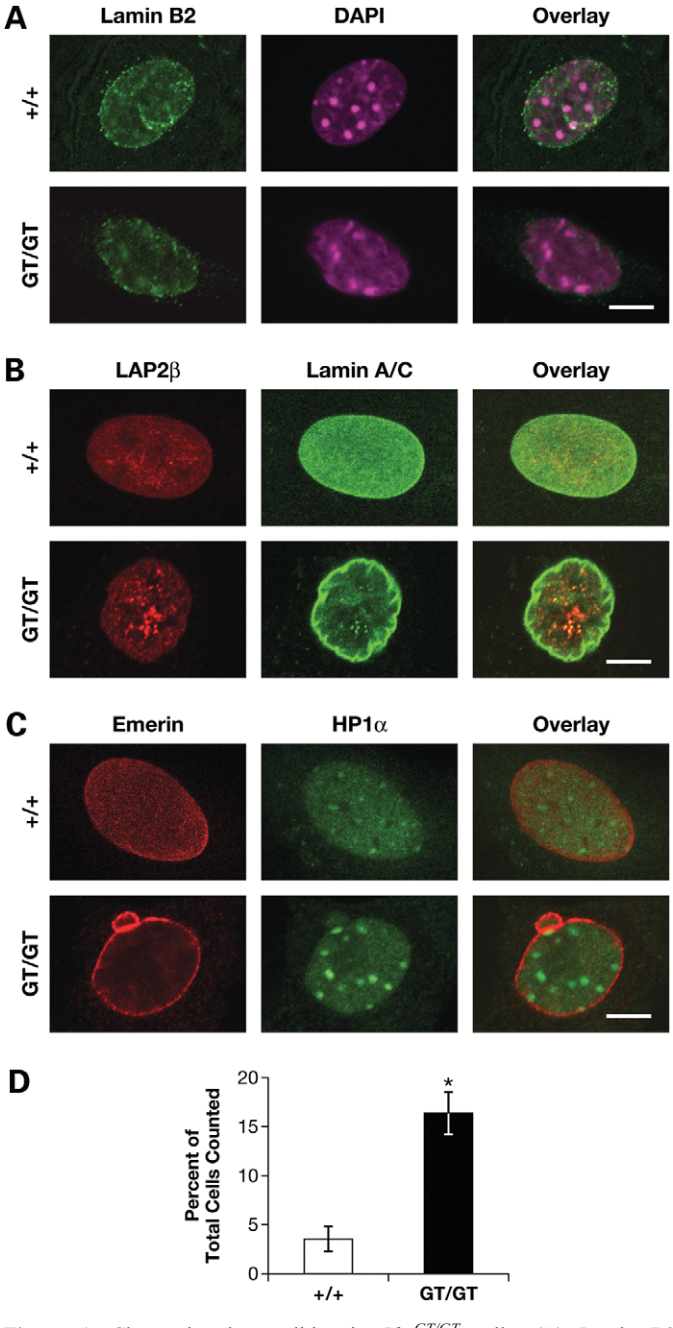

Figure 1. Chromatin abnormalities in $Lbr^{GT/GT}$ cells. (**A**) Lamin B2 expression in the lamina is retained in the $Lbr^{GT/GT}$ cells, although the lamina and NE is wrinkled. (**B**) Similarly, staining for LAP2β and lamin A/C reveal that both are still present in the lamina/NE, although LAP2β also forms inclusions within the nuclei of $Lbr^{GT/GT}$ cells. (**C**) Emerin is also localized at the NE and is strongly localized to a micronucleus whose numbers are increased in $Lbr^{GT/GT}$ cells. Immunofluorescent staining for HP1α indicated increased localization to nucleoplasmic foci in $Lbr^{GT/GT}$ cells. Scale bar, 10 μm. (**D**) $Lbr^{GT/GT}$ cells have an increase in the percentage of micronuclei. Bar graphs represent the percentage of micronuclei relative to the total number of wild-type ($n = 254$) and $Lbr^{GT/GT}$ cells ($n = 172$) counted. $^{*}P < 0.001$.

localized to multiple punctate foci within the nucleoplasm. In $Lbr^{GT/GT}$ PMEFs, the foci are larger and fewer in number (Fig. 1C). Intriguingly, immunofluorescent staining for another NE-associated protein, emerin, revealed increased localization to the NE. Micronuclei were also detected at a higher frequency in the $Lbr^{GT/GT}$ PMEFs (Fig. 1C). Quantification revealed a significant increase of nuclei exhibiting micronuclei from 3.53% (± 1.28; $n = 254$ cells counted) in wild-type cells to 16.34% (± 2.53; $n = 172$ cells counted $P < 0.001$) of $Lbr^{GT/GT}$ PMEFs (Fig. 1D). Interestingly, cells containing micronuclei did not show wrinkling of the lamina, suggesting that micronuclei or wrinkling may be two possible outcomes of the mutation.

Embryonic and tissue specific expression of *Lbr*

The embryonic and tissue-specific expression of *Lbr* was initially determined by the northern analysis (Fig. 2). In embryonic tissues, *Lbr* transcripts were detected at all stages from E4.5 through E18.5, with the levels increasing after E8.5 (Fig. 2A, left panel). *Lbr* transcripts were also present in all adult tissues examined with highest levels in thymus, spleen and testis (Fig. 2A, right panel). The β-galactosidase activity of the gene-trapped fusion protein was used to further localize the expression of *Lbr* in embryonic and post-natal mice. LacZ expression in E10 homozygote embryos was observed at the central nervous system, head and somites (Fig. 2B). In post-natal mice, the expression of *Lbr-lacZ* was observed in the skin where the expression was localized to the hair follicles, specifically in the outer root sheath and more internally in the matrix cells, the highly proliferative cells which give rise to the inner root sheath and hair shaft (25) (Fig. 2C). Expression was also observed in the osteogenic cells of the ulna, femur, ribs and skull (Fig. 2D), with positively stained cells also being observed in the bone marrow.

Lethality of the $Lbr^{GT/GT}$ mutation

Heterozygous intercrosses of $Lbr^{GT/+}$ mice produced viable homozygous mutant offspring. However, the $Lbr^{GT/GT}$ homozygotes were born at a frequency of 11.42% (50 out of 438 mice), indicating that ∼54% of the $Lbr^{GT/GT}$ homozygotes were pre-/peri-natal lethals (Table 1). Examination of embryos from pregnant dams failed to identify abnormal $Lbr^{GT/GT}$ post-implantation embryos, suggesting that embryonic lethality probably occurred during early development, before implantation (data not shown).

Of the live-born offspring, the $Lbr^{GT/GT}$ mice could be easily distinguished by the absence of hair except for a few small patches (Fig. 3A, left panel). The $Lbr^{GT/GT}$ homozygotes were smaller than their wild-type littermates and often exhibited syndactyly between the second and third digits (Fig. 3A, right panel), although with incomplete penetrance. The mean lifespan of the $Lbr^{GT/GT}$ mice was approximately 2–4 weeks (Fig. 3B), with ∼50% dying during the first 3 days after birth. The majority of the remaining $Lbr^{GT/GT}$ homozygotes died in the first 4 weeks, although ∼20% survived until about 10–11 weeks. Homozygotes from the first six generations appeared to survive longer, suggesting that viability maybe influenced by the background strain (the founding mice were C57Bl6/Cr × 129Ola F1 hybrids). The few (6) mice that survived, lived up to 9 months at which time they developed enlarged lymph nodes that resulted in sores

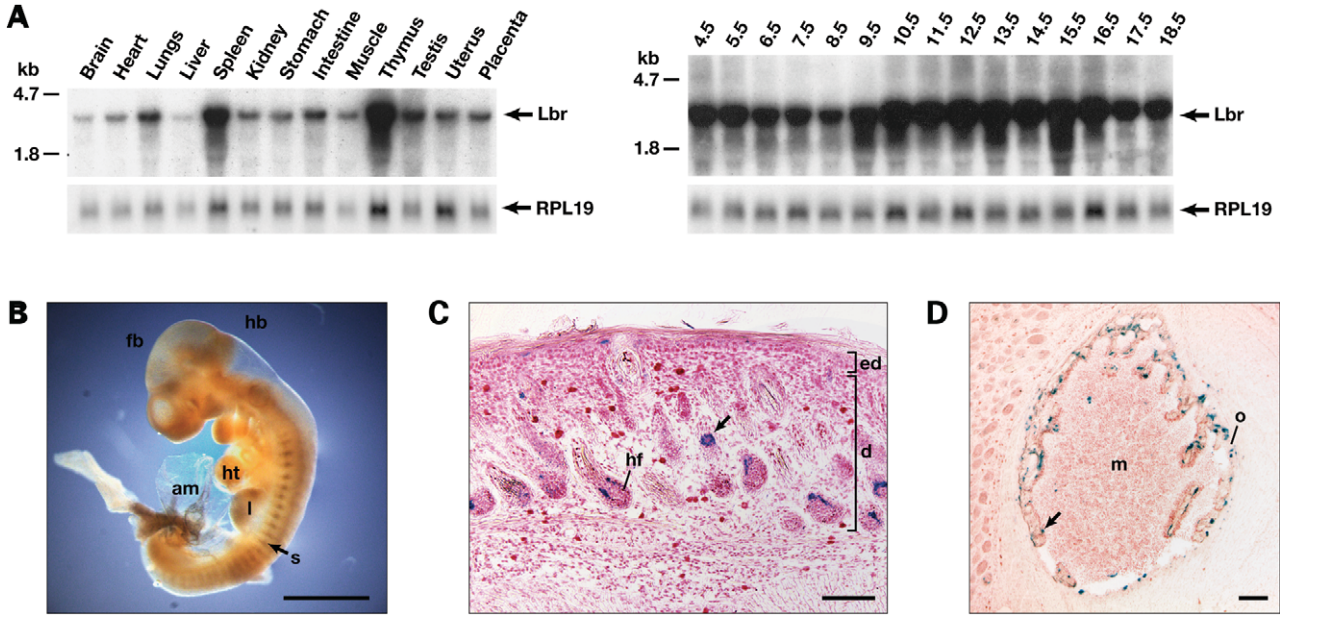

Figure 2. Analysis of the expression of *Lbr*. (**A** Northern blots showing the expression of *Lbr* in embryos (left) and adult tissues (right). (**B**) β-galactosidase staining of an E10 $Lbr^{GT/GT}$ embryo showing expression in the brain, limb buds and somites. fb, forebrain; hb, hindbrain; ht, heart; s, somite; am, amnion. (**C**) Skin section of a 2-week-old post-natal $Lbr^{GT/GT}$ stained with X-gal and counterstained with neutral red showing the expression of *lacZ* in the hair follicles. (**D**) Cross-section through the femoral bone in a 2-week-old post-natal $Lbr^{GT/GT}$ showing expression of *lacZ* in the spongy bone. d, dermis; e, epidermis; hf, hair follicle, ors, outer root sheath. Scale bar = 1 mm (B), 50 μm (C and D).

Table 1. Analysis of progeny from heterozygous ($Lbr^{GT/+}$) intercrosses present at 3 weeks postpartum

	Genotype					
	+/+	GT/+	GT/GT	Total	χ^2	*P*-value
	160 (110)	228 (219)	50 (110)	438	55.99	<0.001 (2 df)
%	11.42 (25)	52.05 (50)	36.53 (25)	100		

Observed numbers of progeny of each genotype are indicated and expected numbers, based on Mendelian ratio 1:2:1, are in parentheses.

necessitating sacrifice of the animal. After the first 6 generations, however, no mice survived longer than 4 weeks.

$Lbr^{GT/GT}$ mice have multiple pathologies

The skin of $Lbr^{GT/GT}$ mice was hyperkeratotic (arrow, Fig. 4A) with little subcutaneous fat. Within the brain, enlarged lateral ventricles were present indicative of hydrocephalus (Fig. 4Ad). Histological analysis with an anti-GFAP antibody, a marker of gliosis, showed increased GFAP positive astrocytes at the periphery and extending out from the ventricles (arrow, Fig. 4Af) and TUNEL staining indicated increased apoptosis within the CNS of $Lbr^{GT/GT}$ mice (data not shown). The nasolacrimal ducts were also clogged with some undefined matter (Fig. 4Ah). The mice were sexually immature with uterine hypoplasia in females (data not shown). Attempts to breed the homozygotes were unsuccessful, indicating infertility. Neither homozygous males nor homozygous females produced litters when intercrossed with

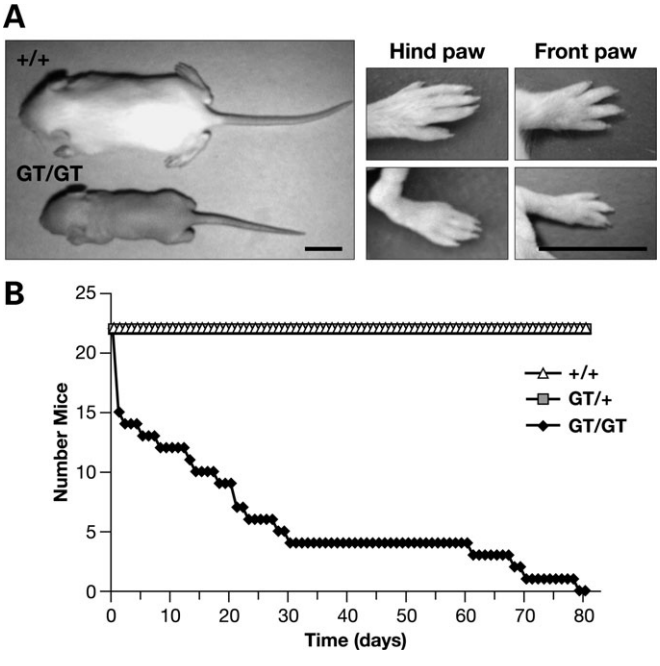

Figure 3. Phenotype of $Lbr^{GT/GT}$ mice. (**A**) $Lbr^{GT/GT}$ and wild-type littermate showing the $Lbr^{GT/GT}$ to have alopecia and a smaller size. Hind paws showing syndactyly between digits 3 and 4. Scale bar, 1 mm. (**B**) *The* $Lbr^{GT/GT}$ also have increased post-natal mortality. GT/GT, homozygote, GT/+, heterozygote, +/+, wild-type.

heterozygous or wild-type mice. For this reason, the colony was maintained by heterozygous matings.

We analyzed the skeletons of post-natal $Lbr^{GT/GT}$ mice following Alazarin red–Alcian blue staining (Fig. 4B). One

major difference between wild-type and $Lbr^{GT/GT}$ mice was a significant bulging of the skull calvaria, although it was unclear whether the abnormal shape was a consequence of hydrocephaly. Scoliosis of the spine was also noted and the rib cage was more compressed resulting in seven lumbar vertebrae between the rib cage and pelvis, whereas there are only six vertebrae in this region in wild-type mice (Fig. 4B). These data together with expression of LBR in bone indicates that LBR has a significant role in skeletal development which will be reported in detail elsewhere (K. Hoffmann, personal communication). Overall, the phenotype of the $Lbr^{GT/GT}$ mice is similar to that described for the ic^{J} mice (18).

Analysis of the hematopoietic lineages

Mutations within the *LBR* affect the nuclear morphology of granulocyte/neutrophils (18,19). In the spleens of wild-type mice, chromatin is uniformly distributed in the nuclei of lymphocytes. In contrast, the splenic lymphocytes of $Lbr^{GT/GT}$ mice were visibly different with clumping of chromatin in the nuclei of lymphocytes (Fig. 4C). Examination of blood smears revealed that granulocyte nuclei were hyposegmented. The nuclei of neutrophils from heterozygous mice were segmented and contained several chromatin clumps. In contrast, the neutrophils from $Lbr^{GT/GT}$ mice contained one large clump, with no nuclear segmentation (Fig. 4Cd and f). Overall, the nuclear morphologies from the hematopoietic tissues of $Lbr^{GT/GT}$ mice were similar those of the ic^{J} mice (18).

To determine the effects of the $Lbr^{GT/GT}$ mutation on hematopoietic lineages, we examined myeloid, erythroid and lymphoid populations by FACS analysis. Examination of cytospins of bone marrow also showed an increase in granulocyte numbers with absence of mature ring forms (Fig. 5A, top panel). Examination of the myeloid lineage, using the markers Gr-1 and Mac-1, revealed an increase in myeloid numbers in the bone marrow ($20.3 \pm 0.8\%$ $Lbr^{+/+}$; $34.7 \pm 5.1\%$ $Lbr^{GT/GT}$) ($P \leq 0.14$), spleen ($7.6 \pm 0.4\%$ $Lbr^{+/+}$; $12.2 \pm 3.3\%$ $Lbr^{GT/GT}$) ($P \leq 0.25$) and peripheral blood ($15.9 \pm 1.2\%$ $Lbr^{+/+}$; $40.3 \pm 4.3\%$ $Lbr^{GT/GT}$) ($P < 0.07$) (Fig. 5A, lower panels). Although the increases were not statistically significant due to the low number of homozygotes available for analysis ($n = 2$), the trend for increased numbers of Mac-1+Gr-1+ cells may be the result of an increased demand for mature neutrophils, as these mice accumulate aberrant neutrophils.

To determine whether lymphoid populations were affected, we examined B cells using markers for progenitors (CD43) and mature B cells (IgM and B220). Although there appeared to be a decrease in immature B cells (B220+CD43-) in $Lbr^{GT/GT}$ mice (18.9 ± 2.3) compared to $Lbr^{+/+}$ mice (35.6 ± 1.0) ($P = 0.05$) (Fig. 5B), the number of mature IgM+ cells from the $Lbr^{GT/GT}$ mice (6.8 ± 1.5) did not differ from wild-type levels (7.8 ± 0.3) ($P = 0.4$) (data not shown). Similarly, there were no differences in erythrocyte levels evident by the numbers of Ter119 and CD71+ve cells (Fig. 5C) and T cells in the $Lbr^{GT/GT}$ mice (data not shown). These data indicate that the most profound effect of the $Lbr^{GT/GT}$ mutation on hematopoietic lineages is on the granulocyte-neutrophil compartment.

LBR is transcriptionally regulated by the granulocyte differentiation factor C/EBPε

Granulocyte differentiation is initiated in Gr-1+ and Mac-1+ myeloblasts. These sequentially differentiate into promyelocytes, myelocytes, metamyelocytes, band granulocytes and finally into mature segmented granulocytes (26). Our analysis showed that the granulocyte nuclei of the $Lbr^{GT/GT}$ were hyposegmented and therefore potentially arrested in their differentiation. We therefore determined at which step the block in granulocyte maturation occurs and whether the granulocytes from the $Lbr^{GT/GT}$ mice were functional.

We noted similarities between the granulocyte morphologies of the $Lbr^{GT/GT}$ mice and humans lacking a functional CCAAT/enhancer binding protein epsilon (C/EBPε) transcription factor (27). Granulocyte differentiation is critically dependent on the CCAAT/enhancer binding protein transcription factors alpha and epsilon (C/EBPα and C/EBPε), with mice deficient in C/EBPε showing marked defects in granulocyte development and increased susceptibility to infection (28–30). Mutations in the *CEBPE* gene are detected in a subset of individuals with neutrophil-specific granule deficiency (SGD), a rare congenital disorder associated with immunodeficiency and neutrophil abnormalities (31). These and other studies have revealed that C/EBPε is essential for the later stages of granulocyte differentiation, specifically with the differentiation of metamyelocytes into banded myelocytes (26).

The morphological similarities in the immature granulocytes between the $Lbr^{GT/GT}$ and the C/EBPε mice prompted us to determine whether C/EBPε transcriptionally regulated the *Lbr* gene. To investigate whether C/EBPε might directly regulate *Lbr* gene transcription, we analyzed the sequence of 2 kb region, upstream of the murine *Lbr* trancripional start site. Three putative C/EBPε binding sites were identified centered at positions −1791, −1335 and −837 bp relative to the major transcriptional initiation site (Fig. 6A). Electrophoretic mobility shift assays (EMSA) and antibody supershift assays were performed using the extracts of HEK293 cells transfected with C/EBPε and C/EBPβ to determine whether C/EBPε interacts with these putative binding sites. C/EBPε formed complexes with oligonucleotides containing each putative C/EBP binding site with strongest binding being found with the −1791 site (Fig. 6B, left panel). C/EBPβ, a related member of the C/EBP family, also bound to each site (Fig. 6B, right), as would be expected based on the shared DNA binding specificities of each of the C/EBPs (32).

Next we tested whether C/EBPε could activate the *Lbr* promoter by performing transient transfection assays. HEK293 cells were transfected with luciferase reporter plasmids (−2045lbr-Luc and −890lbr-Luc) containing *Lbr* promoter sequences extending to nucleotides −2045 or −890 and expression vectors (pC/EBPε and pC/EBPβ, encoding either C/EBPε or C/EBPβ and luciferase activities were measured in cell extracts. Co-transfection of C/EBPε resulted in a dose-dependent increase in the activity of the −2045lbr-Luc reporter (Fig. 6C). C/EBPβ also transactivated this promoter in a dose-dependent manner, although C/EBPβ was less potent than C/EBPε. Both C/EBPε and C/EBPβ were less active on the −890lbr-Luc reporter, presumably reflecting the lower number of putative C/EBP binding sites in this con-

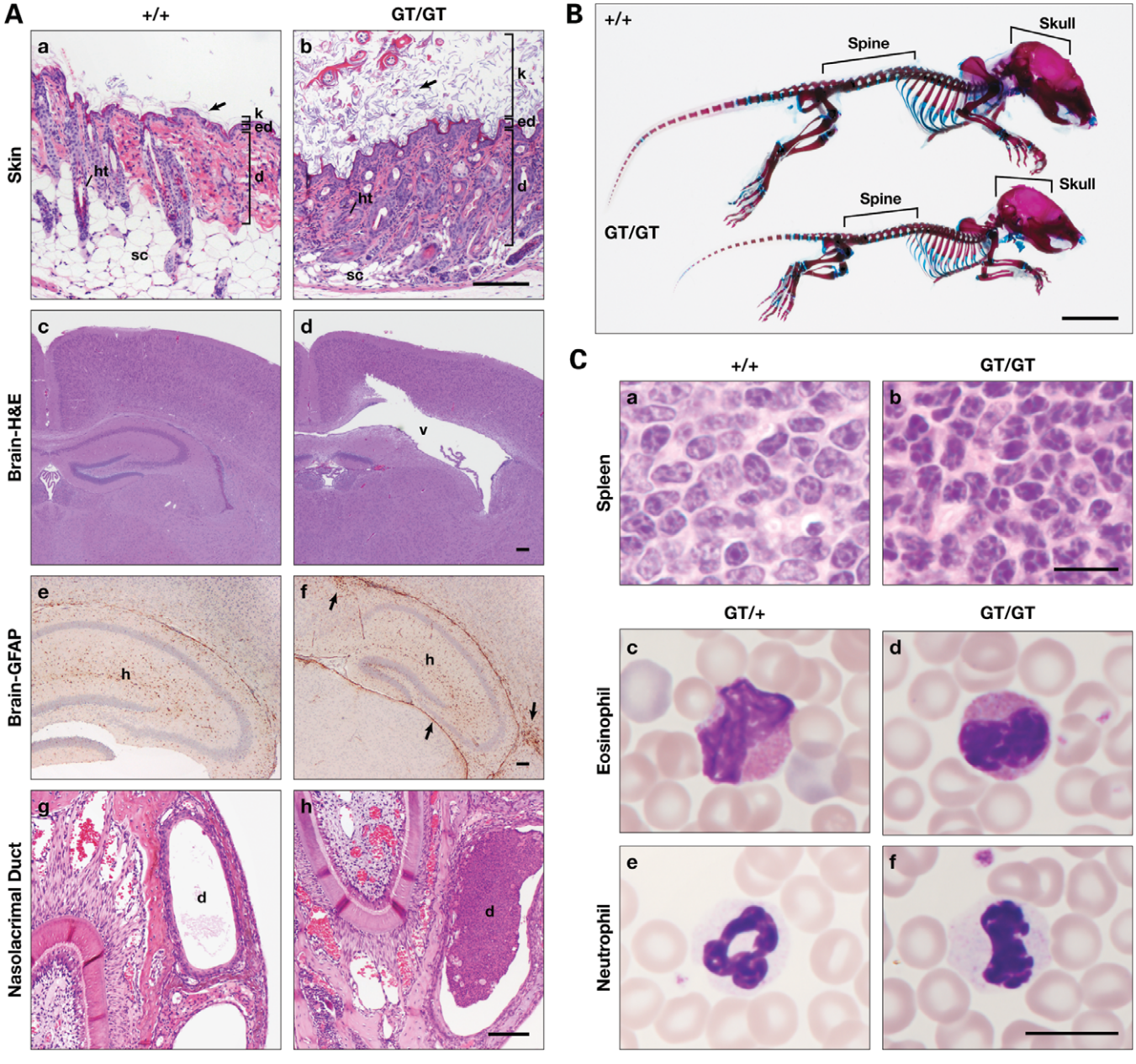

Figure 4. Pathology of the $Lbr^{GT/GT}$ phenotype. (**A**) Hyperkeratinosis in the skin of $Lbr^{GT/GT}$ mice. High-power magnification of a skin section showing an increase in the amount of keratin on the surface of the epidermis. Scale bar = 50 μm d, dermis; ed, epidermis; k, keratin layer; sc, subcutaneous fat. (Ac and d) Hydrocephalus/enlarged ventricles. v, ventricle. (Ae and f) Gliosis in the brain of $Lbr^{GT/GT}$ mice. Brain sections stained with an antibody to GFAP; arrow shows GFAP positive astrocytes in the $Lbr^{GT/GT}$ brain section, indicative of gliosis. (Ag and h) Clogged nasolacrimal duct in $Lbr^{GT/GT}$ mice. (**B**) Skeletons stained with alizarin red and alcian blue showing increased curvature of the spine and a dome-shaped skull in the $Lbr^{GT/GT}$ mice. (**C**a and b) Spleen section showing chromatin clumping. (Cc and d) Eosinophils showing irregular chromatin. (Ce and f) Neutrophils showing the absence of ring forms and nuclear hypo-segmentation in the GT/GT and normal morphology of neutrophils in GT/+ Giemsa–Wright staining. Scale bar = 10 μm.

struct. Together, these results demonstrate that C/EBPε transcriptionally regulates the *Lbr* gene.

Granulocyte function in $Lbr^{GT/GT}$ mice

In mice deficient for C/EBPε, granulocyte development is blocked at the metamyelocyte stage (27) and the mice are functionally unable to counteract infections. Since granulocytes of the $Lbr^{GT/GT}$ mice also had an absence of ring forms, we determined the stage at which differentiation was arrested. We analyzed granule protein expression by real-time PCR for the primary granule marker lactoferrin, the secondary granule marker myeloperoxidase and the tertiary granule marker gelatinase B (MMP9). We found no significant differences between the expression of these proteins in the $Lbr^{GT/GT}$ granulocytes and wild-type controls, with the possible exception of lactoferrin that showed an increase in levels in some of the populations analyzed (Fig. 6D). Since all three stages of

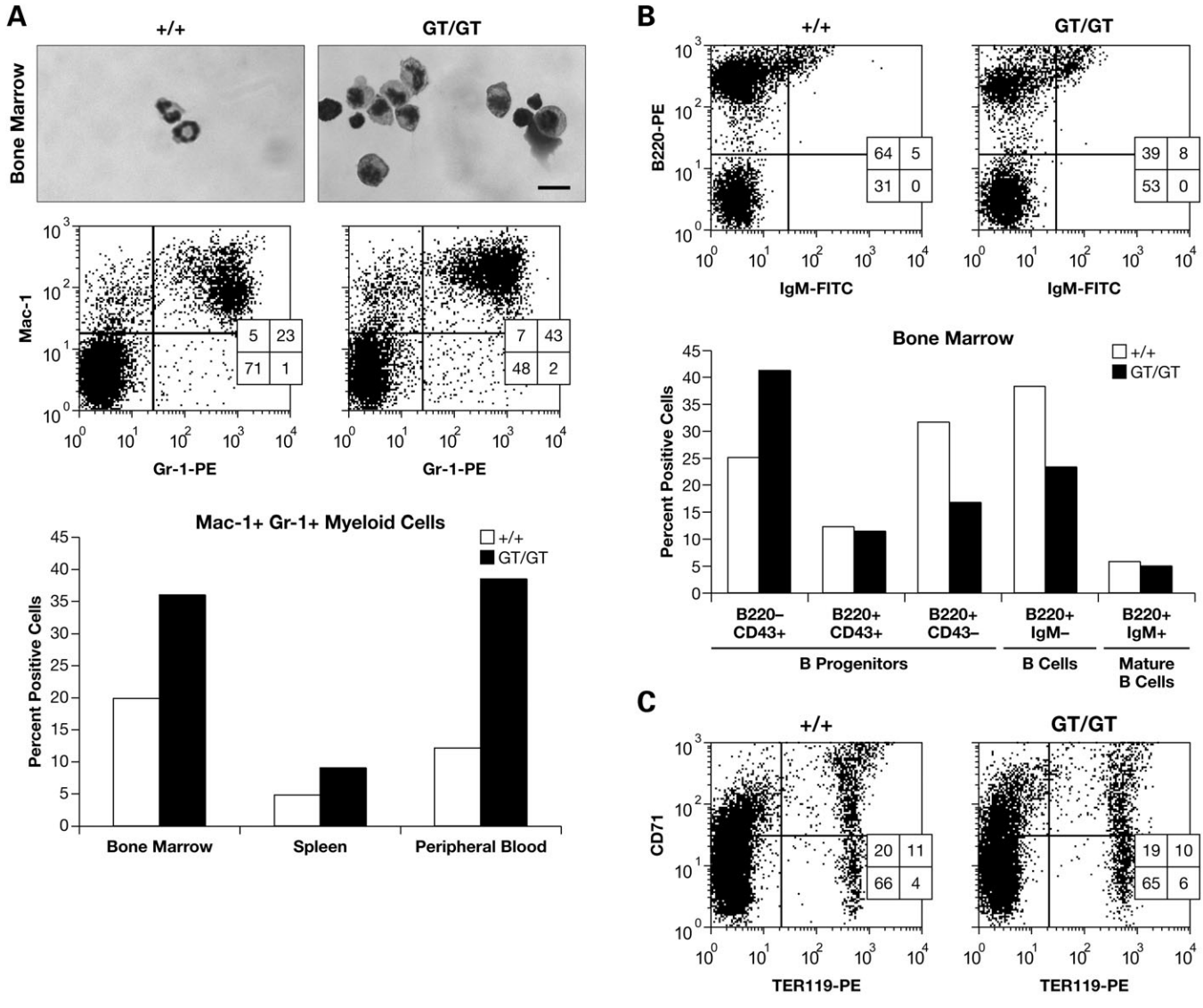

Figure 5. Upregulation of granulocytes in hematopoietic tissues. (**A**) Upper panels show cytospins of bone marrow cells. $Lbr^{+/+}$ cells show ring forms in the nuclei; $Lbr^{GT/GT}$ cells do not show the ring forms. Scale bar= 10 μm. Middle: cells from spleen, bone marrow and peripheral blood were stained with Gr-1 and Mac-1 antibodies to mark myeloid lineages and analyzed by flow cytometry. Bottom: dot blots of spleen samples are representative samples. Graphs represent the average values of upper right quadrants (Mac1+ve, Gr-1+ve) ± SEM of wild-type ($n = 6$) and $Lbr^{GT/GT}$ ($n = 2$) mice. (**B**) Top: dot blots of FACS analysis using markers of B lymphocyte development in the bone marrow and graphs (bottom) representing average values ± SEM; $^{*}P = 0.05$. (**C**) Dot blots of erythrocyte analysis revealing no overt differences. Cells were stained with anti TER-119 and CD-61.

granules are produced in $Lbr^{GT/GT}$ granulocytes, the block to differentiation is likely at a later stage, at which banded granulocytes become segmented. To determine whether the immature $Lbr^{GT/GT}$ granulocytes are still able to counteract infections, we performed a battery of functional tests. We determined that myeloperoxidase and hydrogen peroxide were inducible in the $Lbr^{GT/GT}$ neutrophils (data not shown). We also tested the function of the neutrophils in a *Staphylococcus* killing assay. As shown in Figure 6D, the ability of the $Lbr^{GT/GT}$ neutrophils to kill *Staphylococcus aureus* bacteria did not differ from wild-type controls, indicating that the ability to counteract infection may not be compromised in $Lbr^{GT/GT}$ mice.

Sterol analysis

The C-terminus of LBR contains a domain homologous to sterol reductases (15) and the discovery of abnormal forms of cholesterol in the skin fibroblasts of a human infant with HEM/Greenberg skeletal dysplasia (22) presented an intriguing possibility that abnormalities in cholesterol metabolism may account at least in part for some of the observed phenotype of $Lbr^{GT/GT}$ mice. More recently, however, examination of sterol levels in post-natal ic^{J} mice showed no major differences in cholesterol metabolite levels when compared with their wild-type siblings (23). Specifically, GC/MS analysis of brain cortex sterol levels in 10-day-old

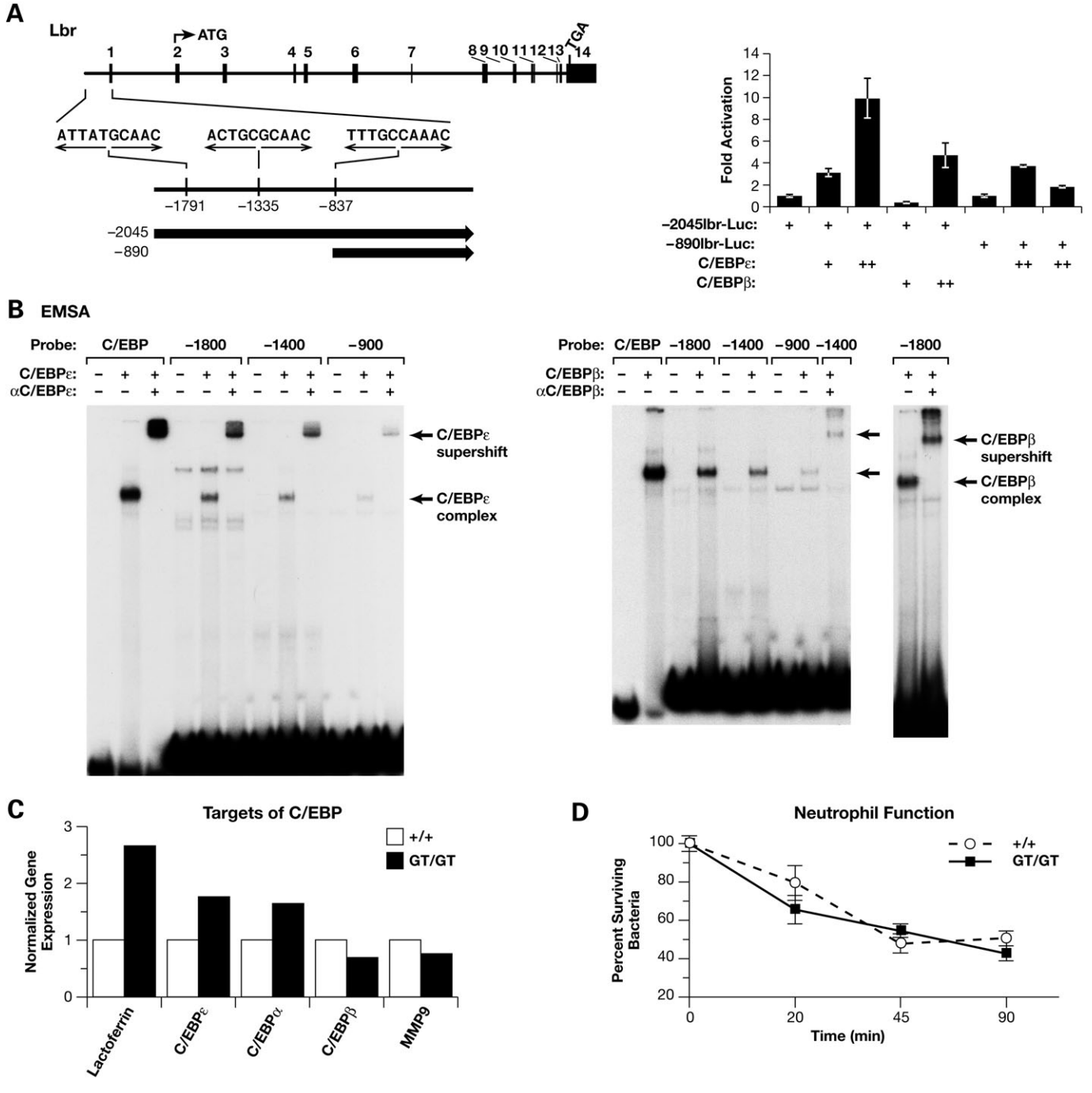

Figure 6. LBR is regulated by C/EBPε. (**A**) Identification of C/EBPε consensus binding sites in the LBR promoter region. Examination of approximately 2000 bp of sequence upstream of the transcriptional start site of the mouse LBR gene revealed three sequences that displayed at least a 6/10 match to the perfect C/EBPε binding site, ATTGCGCAAT (56). (**B**) Characterization of C/EBPε binding sites in the LBR promoter. Nuclear extracts from cells expressing C/EBPε (left panel) or C/EBPβ (right) were analyzed by EMSA for binding to three putative C/EBP sites in the LBR promoter. Binding to a canonical C/EBP site was analyzed for comparison. Where indicated, the appropriate C/EBP antibody was used for supershift analysis. Upper right panel: C/EBPε transactivated the *Lbr* promoter. HEK293 cells were trasfected with 0.5 μg of *Lbr*-luciferase reporter plasmids containing sequences extending to either −2045 or −890 either alone or with 0.5 μg (+) or 1.0 μg (++) of expression vectors encoding C/EBPε or C/EBPβ. Luciferase values were determined 48 h after transfection and expressed as fold increases relative to the reporter plasmid alone. Transfections were performed three times in triplicate and expressed as means ± standard deviations. (**C**) Markers of granulocyte development are not altered in $Lbr^{GT/GT}$ granulocytes. Bone marrow was cultured for 7 days and analyzed by real-time analysis for expression of indicated genes. (**D**) Staph Killing Assay was performed on isolated neutrophils incubated with two *S. aureus*/neutrophil. Data represent the percentage of surviving bacteria of the original bacterial inoculum. Percentage of surviving bacteria in $Lbr^{GT/GT}$ neutrophils is not significantly different from $Lbr^{GT/GT}$ neutrophils ($n = 3$).

post-natals showed a small decrease in cholesterol, unchanged desmosterol levels and a small statistically insignificant increase in cholesta-8,14-dien-3b-ol at post-natal day 1 that decreased to normal levels on days 10 and 21 (23). To determine whether abnormal cholesterol metabolism may account for any of the phenotype of the $Lbr^{GT/GT}$ mice, we also analyzed the sterol content of livers and brains of embryonic $Lbr^{GT/GT}$ mice at E15 by GC-MS. Our analysis did not reveal any differences in cholesterol or desmosterol levels between wild-type and $Lbr^{GT/GT}$ mice and cholesta-8,14-dien-3b-ol levels were not upregulated (data not shown).

DISCUSSION

Heterozygous mutations within the LBR gene (*LBR)* result in the autosomal dominant Pelger–Huët anomaly (18), characterized by hypolobulation of granulocyte nuclei and altered chromatin structure. Homozygous Pelger–Huët anomaly features a more severe blood phenotype and sometimes results in impaired cognitive development, epilepsy, heart defect, skeletal abnormalities and polydactyly (19–21). Homozygous LBR nonsense mutations result in HEM/Greenberg skeletal dysplasia, characterized by *in utero* lethality, characterized by hydrops, short-limbed dwarfism and disorganization of chondro-osseous calcification (with a moth-eaten aspect) and accumulation of cholesterol metabolite cholesta-8,14-dien-3β-ol in skin fibroblasts (22,33). The LBR protein appears to have at least two functional domains. An N-terminal hydrophilic nucleoplasmic domain which interacts with chromatin is also important for NE reassembly (14) and may be involved in RNA processing (34). The C-terminal domain is contained within the eight putative transmembrane motifs and appears to function as a sterol Δ14-reductase or act as a receptor for sterol molecules (15–17), although such functions *in vivo* are somewhat unclear (23). Mutations are found throughout the *LBR* gene, but it has been difficult to assign a specific mutation, resulting in a particular phenotype, that specifically disrupts either one or other domain, as is seen in the laminopathies (3,35).

Here we have characterized a novel line of mice carrying a gene-trap insertion into exon 9 of the *Lbr* gene. This mutation resulted in the formation of a hybrid protein consisting of the first 366 amino acids fused to β-galactosidase and lacking the last four transmembrane domains and the C-terminus. The LBR–β-gal fusion protein was localized to the ER, in contrast to the normal LBR protein, which is localized predominantly to the NE. This redistribution of LBR altered fibroblast nuclear morphology, as well as the localization of other NE-associated proteins. In $Lbr^{GT/GT}$ fibroblasts, many of the nuclei were misshapen, with the NE and lamina having a wrinkled appearance. LAP2β was mislocalized and formed distinct foci within the nucleus. In addition, HP1α was localized to larger granules in $Lbr^{GT/GT}$ fibroblasts, possibly due to the disruption of LBR–HP1 complexes and to chromatin.

Micronuclei were associated with the nucleus in ∼16% of interphase nuclei and the micronuclei were enriched for emerin. Such micronuclei have recently been described in fibroblasts with defective expression of Nesprins 1 and 2 (36). It was suggested that micronuclei were formed as a consequence of incomplete cell division at mitosis, a defect that may also be a consequence of LBR loss, as the LBR is required for NE reassembly after mitosis (14). Interestingly, cells containing micronuclei did not show wrinkling of the lamina, suggesting that micronuclei or wrinking may be two possible outcomes of the mutation. Whether wrinkling results in micronuclei formation or vice versa, however, could not be determined from the data.

Mice heterozygous for the $Lbr^{GT/+}$ insertion are overtly normal, whereas the $Lbr^{GT/GT}$ homozygotes phenocopy ic^{J} mice, exhibiting embryonic lethality with incomplete penetrance, shortened post-natal lifespan, hydrocephalus and syndactyly, as well as chromatin atypia in the neutrophils. The surviving $Lbr^{GT/GT}$ homozygotes had scoliosis and syndactyly. Furthermore, the skull was abnormal with a distinct doming of the parietal bones. This abnormality may have been a consequence of hydrocephalus of the $Lbr^{GT/GT}$ mice that was associated with fluid-filled inclusions within the brain and enlargement of the lateral ventricles. The spine showed increased scoliosis with the rib cage being more compressed resulting in the presence of seven lumbar vertebrae between the rib cage and pelvis, whereas there are six in wild-type mice. A similar phenotype has been reported for the disruption of *Ledgf/Psip* gene (37), another chromatin-associated protein that contains a Tudor domain and which may interact with RNA. Intriguingly, mutations in the human PSIP are also associated with the disruption of hematopoietic lineages with the formation of myeloid leukemias (38).

We extended our comparison of the $Lbr^{GT/GT}$ mice to the ic^{J} mice by showing that in the affected tissues, *Lbr* is not ubiquitously expressed in all cells, but appears to be restricted to a few cell types within each tissue. During embryogenesis, *Lbr* is expressed in the central nervous system and brain. In post-natal skin, *Lbr* expression is localized to the base of the hair follicles, and in the skeletal system, *Lbr* expression was restricted to osteogenic cells in the radius, ulna and ribs. These results indicate that the function of LBR is essential to only a few specific cell types, but when disrupted, results in many tissues showing some form of pathology, e.g. alopecia and hyperkeratosis in the skin.

Embryonic lethality and perhaps some of the more severe effects associated with mutations in the *Lbr* gene have been attributed to the mutations affecting in the putative sterol activity of the LBR protein. However, when we analyzed sterol levels in the brains and livers from E15 $Lbr^{GT/GT}$ embryos, we were unable to find any significant changes in sterol metabolite and cholesterol levels. This result was consistent with a recent report indicating that *DHCR14*, another sterol D14-reductase, may compensate for the loss of LBR in regulating cholesterol synthesis in mice (23). Because we were unable to assay sterol metabolism in the resorbed embryos, we cannot exclude the possibility that sterol metabolism was defective in embryos with incomplete penetrance, resulting in lethality in some individuals but not others or that our methods were insufficient to detect the abnormal metabolites. However, an alternative cause of embryonic lethality may be due to the chromatin-binding activity of LBR.

We observed that some homozygotes died *in utero* beginning at E7, whereas others survived but died peri-natally and later at 3–4 weeks post-natally. It is possible that the defective binding of LBR to HP1α and chromatin could result in epigenetic anomalies resulting in abbreviated development at various stages of embryogenesis. For example, inefficient chromosomal anchorage during mitosis could result in defective gene expression, chromosomal anomalies and defective cell division, resulting in death at different developmental stages. Similarly, embryonic lethality arises in homozygous mutations of the Tudor-containing transcription factor involved in chromatin remodeling, MRG15; developmental delay is observed at E14.5 with some embryos dying perinatally and showing decreased cellular proliferation (39). However, our data cannot validate this hypothesis at present.

Loss of LBR and its consequences on nuclear morphology has been extensively described in hematopoietic lineages (21). As with the *ic*^{J} mice, we noted clumping of the heterochromatin in splenic and thymic populations. The role of LBR in the thymus and spleen, however, is unclear even though expression analysis showed high levels of LBR in these tissues. We did not detect any differences in spleen and thymus cell numbers. However, there may have been a delay in B cell maturation as B220-CD49+ numbers were increased in the bone marrow and mature forms were reduced. We also found no evidence for impaired immune function, a result similar to that previously reported in dogs with Pelger–Huët (40).

The characteristic phenotype associated with Pelger–Huët is in the nuclear morphology of the granulocyte/neutrophil lineage. Granulocyte/neutrophil maturation is characterized by a sequential set of morphological changes in which myeloblasts differentiate from promyelocytes to metamyelocytes to banded granulocytes to mature granulocytes. These stages are marked by changes in nuclear morphology with the cells initially having a single monolobulated nucleus which progresses to a banded ring-form nucleus and then to a multilobulated nucleus. Such changes are accompanied by increases in the primary, secondary and tertiary granule proteins (26).

We noted similarities in the abnormal neutrophil nuclear morphology between the C/EBPε null mice and the *Lbr*$^{GT/GT}$ mice, suggesting a potential interaction between the two nuclear factors. There are six members of the CEBP family, α, β, γ, ∂, ε and ζ, and several are expressed within the hematopoietic system (41). C/EBPα is expressed early in the myeloid lineage and promotes neutrophil differentiation in part by activating the *CEBPE* gene (42). C/EBPε is primarily expressed in myeloid cells and is required for myelocyte differentiation to banded granulocytes (29). Mutations in the *CEBPE* gene in humans are associated with a subset of individuals with SGD (31). Mice deficient in C/EBPε succumb to infections at 2–5 months with the granulocytes being deficient in secondary and tertiary granule proteins, as well as showing reduced expression of the cytokines such as IL-2, and IL-4. Our studies identified three C/EBPε consensus binding sites in the promoter region upstream of the *Lbr* start site. We showed that C/EBPε protein bound to these sites and that C/EBPε transactivated *Lbr*-luciferase reporter plasmids in a pattern dependent on the amount of C/EBPε expression plasmid and the number of C/EBP sites in the reporter plasmid.

The reasons for why nuclear morphology changes during granulopoiesis remain unclear. One possibility is that the changes may reflect a change in the accessibility of genes to transcription factors, with LBR providing chromatin anchoring points (6,43). An alternative suggestion is that the nuclear changes facilitate neutrophil migration into tissues by making the nucleus more deformable, particularly since the increase in LBR expression is not accompanied by an increase in A-type lamin expression that would make the nucleus more rigid (44). An increase in LBR levels is associated with changes in nuclear morphology, with the NE interacting with microtubules by an unknown mechanism, with this interaction resulting in the pulling and folding of the nucleus (44). Loss of LBR may therefore result in the nucleus remaining monolobulated due to a failure in the microtubules to attach to the interphase NE. It would also be of interest to see if monolobulation resulted in defective neutrophil migration through tissues.

Our results indicate that the *Lbr* gene is under transcriptional control of C/EBPε and that this control is a necessary step in the morphological differentiation of the nuclei in the myeloid lineages. How LBR expression is regulated in other tissues is unclear at present. Despite the failure of granulocyte nuclei to undergo morphological change during their differentiation, this did not impair granulocyte functionality. The granulocytes from the *Lbr*$^{GT/GT}$ mice were not defective in producing anti-bactericidal factors or in the killing of *S. aureus* bacteria. However, only one type of gram-positive bacteria (*S. aureus*) was tested. Granulocytes kill gram-positive, gram-negative bacteria and fungi by releasing neutrophil extracellular nets (NETs) (reviewed in (45). Although it is possible that more sophisticated analysis of bacterial killing activity may reveal some differences between wild-type and *Lbr*$^{GT/GT}$ granulocytes, our results suggest that major changes in nuclear morphology may not be essential to granulocyte functionality.

MATERIALS AND METHODS

Generation of *Lbr*$^{GT/GT}$ mice

The ES cell line XE569 containing a gene-trap insertion mutation (24) in the *Lbr* locus was obtained from BayGenomics (http://www.genetrap.org). ES cells were microinjected into C57Bl/6$^{Brd/brd}$ albino blastocysts as described (46). The resulting *Lbr*^{GT} line was maintained as heterozygotes and intercrossed to obtain homozygotes (*Lbr*$^{GT/GT}$). All mice were maintained in our facility in accordance with the procedures outlined in the Guide for the Care and Use of Laboratory Animals (NIH Publication No. 86-23, 1985).

Genotypes were determined by Southern blotting or PCR. For southern analysis, tail DNA was double digested with Asp718, then probed with a 746 bp fragment in the region of exon 6 of the *Lbr* locus, generated with forward primer 5′-GTGTGTCCACTCTTGTCAACC-3′ and reverse primer 5′-ATACTCAAATGTGGATTCAGACTAGC-3′.

For genotyping by PCR, genomic DNA was amplified with forward primer LBR 21614F 5-TTCCTATGGACTGGG TGTGGAG-3′ and reverse primer 5-GCCTGAAACTGGGT CAAATAAGG-3′ to generate a wild-type 702 bp product and

primers LBR 21614F and reverse primer 5′-TCAAACC TGAACCCCGACTTC-3′ to generate a mutant 504 bp product.

Northern analysis

Total RNA was extracted using the RNAeasy Kit (Qiagen, Valencia, CA, USA). Ten micrograms of RNA was separated on 1% formaldehyde agarose gels and transferred to Hybond membranes (Amersham Biotech, Piscataway, NJ, USA). Blots were probed with a *Sal*I–*Eco*RV fragment of an IMAGE. Consortium clone ID 4216442 containing nucleotides 1–228 of the LBR transcript. The mouse *Gapdh* cDNA was used as a loading control. Tissue and embryonic blots were obtained from Seegene, Inc (Rockville, MD, USA).

Derivation of $Lbr^{GT/GT}$ gene-trapped cells

$Lbr^{GT/+}$, GT/GT and wild-type fibroblasts were derived from E13 embryos of heterozygous crosses as described (47). Granulocyte cultures were derived as follows: bone marrow was extracted from the femoral bone and plated in IMDM containing 10% FCS 1% PenStrep and 100 ng/ml of murine SCF (PeproTech, Inc., Rocky Hill, NJ, USA), 50 ng/ml of IL-6 (BioSource, Camarillo, CA, USA) and 50 ng/ml of G-CSF (PeproTech, Inc.) for 7 days.

Embryo analysis and histological staining

Embryos ages E8.0–10.0 were stained for *LacZ* expression and photographed as previously described (47). Embryos and newborn mice were frozen in OCT, and lacZ staining was performed on sections as previously described (47). Embryos at E15 were analyzed for sterol content as described (48); (23).

Tissues fixed in 10% buffered neutral formalin were paraffin-embedded, sectioned at 5μm and stained with hematoxylin and eosin, Apop Tag (TUNEL) and GFAP (Dako Cytomation). Skeletons were stained with Alizarin red and Alcian blue stain for bone and cartilage using standard methods (49).

Flow cytometry

Cell suspensions were prepared from peripheral blood, bone marrow, thymus and spleen of 3-week-old mice. Cells were blocked in PBS containing 0.1% bovine serum albumin (sort buffer) at a concentration of 2×10^7 cells/ml in a volume of 100 μl. Cells were incubated with indicated mixtures fluorochrome-conjugated primary antibodies in sort buffer: Gr-1, Mac-1, IgM, B220, CD43, Thy1.2, CD 4, CD8, TER119 and CD71 for 30 min at 4°C. Cells were washed and resuspended in sort buffer for FACS analysis. Cytospins were prepared using the Three-Step Stain Set (Richard-Allan Scientific, Kalamazoo, MI, USA) according to manufacturer's instructions.

Immunostaining and immunoblotting

PMEFs were fixed with 4% paraformaldehyde, stained with primary antibodies to lamin A/C (sc-6215), LAP2β (a kind gift from Roland Foisner), emerin (Novocastra), β-galactosidase (Chemicon) and then with secondary antibodies conjugated to Alexa488 or Alexa568 (Molecular Probes, Eugene, OR, USA). After immunolabeling, cover slips were mounted in Vectashield Mounting Medium (Vector Laboratories, Burlingame, CA, USA) and visualized using a Zeiss Axiophot inverted microscope.

Western blotting was performed on PMEF whole cell lysates as described (50) using an anti-LBR antibody (kind gift of Herald Hermann).

Real-time PCR

RNA was prepared from bone marrow samples using the RNAeasy MiniKit (Qiagen). Oligonucleotides for target genes were for C/EBPε, α and β, MMP9 (gelatinase B) (Supplementary Material, Table S2). PCR was performed as described in (50) on an ABI Prism cycler. Raw Ct values were normalized to GAPDH and HPRT and relative gene expression was obtained using the $\Delta\Delta C_T$ method (51).

Promoter analysis

EMSA was performed essentially as described (52) using double-stranded probes (Supplementary Material, Table S1) corresponding to the indicated regions of the LBR promoter or containing a canonical C/EBP site (52). C/EBPε and C/EBPβ were expressed in transfected HEK293 cells, and nuclear extracts (0.5 μg) were analyzed by EMSA.

Sequences containing *Lbr* promoter fragments with 5′ coordinates at −2045 and −890 were PCR-amplified from mouse genomic DNA and inserted into the pGL3-luc reporter plasmid (Promega) using primers ATATCCCGGGTTTCTGGACTCTGAGAGCATCC and GCCGGTACCCGCAGGACTCGGAGTAGGATTCGT and the reverse primer ATATCCCGGGC ACTCCAGGACAGTCACCAG. *Sma*I and *Kpn*I sites used for subcloning are underlined within the primer sequences. The proofreading thermostable polymerase *Pfu* was used in PCR reactions and PCR products were sequenced to ensure that no unintended sequence alterations were introduced. HEK293 cells were obtained from the American Type Culture Collection (Manassas, VA, USA) and were maintained in Dulbecco's Modified Eagle's Medium (BioWhittaker, Frederick, MD, USA) supplemented with 10% fetal bovine serum (Hyclone, Logan, UT, USA). HEK 293 cells were transfected using Effectene reagent (Qiagen) with 0.5 μg of reporter plasmid and 0.5 or 1.0 μg of either pMEX Flag-C/EBPε or pMEX Flag-C/EBPβ (53). Cells were harvested 48 h after transfection and luciferase activities were assayed using the Luciferase Assay Kit (Promega).

Functional activity of murine neutrophils

The presence of myeloperoxidase in murine neutrophils was demonstrated histochemically using Kaplow's stain (54). To assess hydrogen peroxide production, murine neutrophils were incubated with phorbol myristate acetate (100 ng/ml, Sigma-Aldrich Co., St Louis, MO, USA) for 30 min at 37°C in a slide chamber (Lab-Tek, Nalge Nunc International, Rochester, NY, USA) in the presence of Nitroblue tetrazolium (0.1%, Sigma-Aldrich Co.). The neutrophils, which settled on the slide, were counterstained with 0.1% safranin

(Sigma-Aldrich Co.) and examined microscopically. Neutrophil hydrogen peroxide production converted the soluble Nitroblue tetrazolium to insoluble, blue–black formazan deposits on the neutrophils.

To assay bactericidal activity, *S. aureus*, substrain 502A (American Type Culture Collection) was suspended in trypticase soy broth (Becton, Dickinson and Co., Franklin Lakes, NJ, USA) and grown in a shaker water bath at 37°C until the bacteria were in log phase. The bacteria were spun at 2500 r.p.m. (Epppendorf Microfuge) at 4°C for 5 minutes, washed twice with Hanks' balanced salt solution (HBSS) without divalent cations and then resuspended in HBSS. The bacterial cell concentration was adjusted using the optical density (an $OD_{650} = 0.250$ yields $0.8-1 \times 10^8$ bacteria/ml). Bacteria (two bacteria/neutrophil) were added to the murine neutrophils (5×10^6 ml^{-1}) in the presence of freshly harvested murine serum (10%). The cells were incubated for 90 min at 37°C on an end-over-end rotator. Control reactions with bacteria and serum alone were included in the study to exclude the possibility of serum bactericidal activity. At the indicated times, an aliquot of the neutrophil suspension was lysed in distilled water (10 ml) to release the viable bacteria. A known fraction of the lysate was added to a 60×15 mm tissue culture dish (Becton, Dickinson and Co.), mixed thoroughly with warm, trypticase soy agar (Becton, Dickinson and Co.) and then allowed to solidify. The plates were incubated for 48 h in a 37°C dry incubator to allow for colony formation. Colony formation was enumerated using image analysis software (Image-Pro Plus, Media Cybernetics, Inc., Bethesda, MD, USA). The data are the number of surviving bacteria as a percentage of the original bacterial inoculum (55).

SUPPLEMENTARY MATERIAL

Supplementary Material is available at HMG Online.

FUNDING

This research was supported in part by the Intramural Research Program of the NIH, National Cancer Institute, Center for Cancer Research, and with Federal funds from the National Cancer Institute, National Institutes of Health, under Contract No. NO1-CO-12400.

ACKNOWLEDGEMENTS

The authors would like to thank F. Denny Porter and Christopher Wassif for help with sterol analysis of the *Lbr*$^{GT/GT}$ mice, Richard Frederickson for preparation of the figures and Teresa Sullivan for technical assistance.

Conflict of Interest statement. The authors report no conflict of interest.

NOTE ADDED IN PROOF

While this manuscript was in preparation an article appeared online describing similar investigations on granulocyte function from icj mice. Gaines, P., *et al. Exp Hematol.*, 2008.

REFERENCES

1. Stewart, C.L., Roux, K.J. and Burke, B. (2007) Blurring the boundary: the nuclear envelope extends its reach. *Science*, **318**, 1408–1412.
2. Dechat, T., Pfleghaar, K., Sengupta, K., Shimi, T., Shumaker, D.K., Solimando, L. and Goldman, R.D. (2008) Nuclear lamins: major factors in the structural organization and function of the nucleus and chromatin. *Genes Dev.*, **22**, 832–853.
3. Worman, H.J. and Bonne, G. (2007) 'Laminopathies': a wide spectrum of human diseases. *Exp. Cell. Res.*, **313**, 2121–2133.
4. Schirmer, E.C. and Foisner, R. (2007) Proteins that associate with lamins: many faces, many functions. *Exp. Cell Res.*, **313**, 2167–2179.
5. Worman, H.J., Yuan, J., Blobel, G. and Georgatos, S.D. (1988) A lamin B receptor in the nuclear envelope. *Proc. Natl Acad. Sci. USA*, **85**, 8531–8534.
6. Pyrpasopoulou, A., Meier, J., Maison, C., Simos, G. and Georgatos, S.D. (1996) The lamin B receptor (LBR) provides essential chromatin docking sites at the nuclear envelope. *EMBO J.*, **15**, 7108–7119.
7. Simos, G. and Georgatos, S.D. (1992) The inner nuclear membrane protein p58 associates in vivo with a p58 kinase and the nuclear lamins. *EMBO J.*, **11**, 4027–4036.
8. Simos, G. and Georgatos, S.D. (1994) The lamin B receptor-associated protein p34 shares sequence homology and antigenic determinants with the splicing factor 2-associated protein p32. *FEBS Lett.*, **346**, 225–228.
9. Nikolakaki, E., Meier, J., Simos, G., Georgatos, S.D. and Giannakouros, T. (1997) Mitotic phosphorylation of the lamin B receptor by a serine/arginine kinase and p34(cdc2). *J. Biol. Chem.*, **272**, 6208–6213.
10. Ye, Q. and Worman, H.J. (1996) Interaction between an integral protein of the nuclear envelope inner membrane and human chromodomain proteins homologous to Drosophila HP1. *J. Biol. Chem.*, **271**, 14653–14656.
11. Martins, S.B., Eide, T., Steen, R.L., Jahnsen, T., Skalhegg, B.S. and Collas, P. (2000) HA95 is a protein of the chromatin and nuclear matrix regulating nuclear envelope dynamics. *J. Cell Sci.*, **113** (Pt 21), 3703–3713.
12. Simos, G., Maison, C. and Georgatos, S.D. (1996) Characterization of p18, a component of the lamin B receptor complex and a new integral membrane protein of the avian erythrocyte nuclear envelope. *J. Biol. Chem.*, **271**, 12617–12625.
13. Braunagel, S.C., Williamson, S.T., Ding, Q., Wu, X. and Summers, M.D. (2007) Early sorting of inner nuclear membrane proteins is conserved. *Proc. Natl Acad. Sci. USA*, **104**, 9307–9312.
14. Ma, Y., Cai, S., Lv, Q., Jiang, Q., Zhang, Q., Sodmergen, Zhai, Z. and Zhang, C. (2007) Lamin B receptor plays a role in stimulating nuclear envelope production and targeting membrane vesicles to chromatin during nuclear envelope assembly through direct interaction with importin beta. *J. Cell Sci.*, **120**, 520–530.
15. Silve, S., Dupuy, P.H., Ferrara, P. and Loison, G. (1998) Human lamin B receptor exhibits sterol C14-reductase activity in Saccharomyces cerevisiae. *Biochim. Biophys. Acta*, **1392**, 233–244.
16. Bennati, A.M., Castelli, M., Della Fazia, M.A., Beccari, T., Caruso, D., Servillo, G. and Roberti, R. (2006) Sterol dependent regulation of human TM7SF2 gene expression: role of the encoded 3beta-hydroxysterol Delta14-reductase in human cholesterol biosynthesis. *Biochim. Biophys. Acta*, **1761**, 677–685.
17. Holmer, L., Pezhman, A. and Worman, H.J. (1998) The human lamin B receptor/sterol reductase multigene family. *Genomics*, **54**, 469–476.
18. Shultz, L.D., Lyons, B.L., Burzenski, L.M., Gott, B., Samuels, R., Schweitzer, P.A., Dreger, C., Herrmann, H., Kalscheuer, V., Olins, A.L. *et al.* (2003) Mutations at the mouse ichthyosis locus are within the lamin B receptor gene: a single gene model for human Pelger–Huet anomaly. *Hum. Mol. Genet.*, **12**, 61–69.
19. Hoffmann, K., Dreger, C.K., Olins, A.L., Olins, D.E., Shultz, L.D., Lucke, B., Karl, H., Kaps, R., Muller, D., Vaya, A. *et al.* (2002) Mutations in the gene encoding the lamin B receptor produce an altered nuclear morphology in granulocytes (Pelger–Huet anomaly). *Nat. Genet.*, **31**, 410–414.
20. Oosterwijk, J.C., Mansour, S., van Noort, G., Waterham, H.R., Hall, C.M. and Hennekam, R.C. (2003) Congenital abnormalities reported in Pelger–Huet homozygosity as compared to Greenberg/HEM dysplasia: highly variable expression of allelic phenotypes. *J. Med. Genet.*, **40**, 937–941.
21. Hoffmann, K., Sperling, K., Olins, A.L. and Olins, D.E. (2007) The granulocyte nucleus and lamin B receptor: avoiding the ovoid. *Chromosoma*, **116**, 227–235.
22. Waterham, H.R., Koster, J., Mooyer, P., Noort Gv, G., Kelley, R.I., Wilcox, W.R., Wanders, R.J., Hennekam, R.C. and Oosterwijk, J.C.

(2003) Autosomal recessive HEM/Greenberg skeletal dysplasia is caused by 3 beta-hydroxysterol delta 14-reductase deficiency due to mutations in the lamin B receptor gene. *Am. J. Hum. Genet.*, **72**, 1013–1017.
23. Wassif, C.A., Brownson, K.E., Sterner, A.L., Forlino, A., Zerfas, P.M., Wilson, W.K., Starost, M.F. and Porter, A.F. (2007) HEM dysplasia and ichthyosis are likely laminopathies and not due to 3{beta}-hydroxysterol {Delta}14-reductase deficiency. *Hum. Mol. Genet*, **16**, 1176–1187.
24. Skarnes, W. (1990) Entrapment vectors: a new tool for mammalian genetics. *Biotechnology (NY)*, **8** (9), 827–831.
25. Rhee, H., Polak, L. and Fuchs, E. (2006) Lhx2 maintains stem cell character in hair follicles. *Science*, **312**, 1946–1949.
26. Lekstrom-Himes, J.A. (2001) The role of C/EBP(epsilon) in the terminal stages of granulocyte differentiation. *Stem Cells*, **19**, 125–133.
27. Lekstrom-Himes, J. and Xanthopoulos, K.G. (1999) CCAAT/enhancer binding protein epsilon is critical for effective neutrophil-mediated response to inflammatory challenge. *Blood*, **93**, 3096–3105.
28. Williams, S.C., Du, Y., Schwartz, R.C., Weiler, S.R., Ortiz, M., Keller, J.R. and Johnson, P.F. (1998) C/EBPepsilon is a myeloid-specific activator of cytokine, chemokine, and macrophage-colony-stimulating factor receptor genes. *J. Biol. Chem.*, **273**, 13493–13501.
29. Yamanaka, R., Barlow, C., Lekstrom-Himes, J., Castilla, L.H., Liu, P.P., Eckhaus, M., Decker, T., Wynshaw-Boris, A. and Xanthopoulos, K.G. (1997) Impaired granulopoiesis, myelodysplasia, and early lethality in CCAAT/enhancer binding protein epsilon-deficient mice. *Proc. Natl Acad. Sci. USA*, **94**, 13187–13192.
30. Verbeek, W., Wachter, M., Lekstrom-Himes, J. and Koeffler, H.P. (2001) C/EBPepsilon −/− mice: increased rate of myeloid proliferation and apoptosis. *Leukemia*, **15**, 103–111.
31. Lekstrom-Himes, J.A., Dorman, S.E., Kopar, P., Holland, S.M. and Gallin, J.I. (1999) Neutrophil-specific granule deficiency results from a novel mutation with loss of function of the transcription factor CCAAT/enhancer binding protein epsilon. *J. Exp. Med.*, **189**, 1847–1852.
32. Williams, S.C., Cantwell, C.A. and Johnson, P.F. (1991) A family of C/EBP-related proteins capable of forming covalently linked leucine zipper dimers *in vitro*. *Genes Dev.*, **5**, 1553–1567.
33. Konstantinidou, A., Karadimas, C., Waterham, H.R., Superti-Furga, A., Kaminopetros, P., Grigoriadou, M., Kokotas, H., Agrogiannis, G., Giannoulia-Karantana, A., Patsouris, E. *et al.* (2008) Pathologic, radiographic and molecular findings in three fetuses diagnosed with HEM/Greenberg skeletal dysplasia. *Prenat. Diagn.*, **28**, 309–312.
34. Nikolakaki, E., Drosou, V., Sanidas, I., Peidis, P., Papamarcaki, T., Iakoucheva, L.M. and Giannakouros, T. (2008) RNA association or phosphorylation of the RS domain prevents aggregation of RS domain-containing proteins. *Biochim. Biophys. Acta*, **1780**, 214–225.
35. Burke, B. and Stewart, C.L. (2006) The laminopathies: the functional architecture of the nucleus and its contribution to disease. *Annu. Rev. Genomics Hum. Genet.*, **7**, 369–405.
36. Zhang, Q., Bethmann, C., Worth, N.F., Davies, J.D., Wasner, C., Feuer, A., Ragnauth, C.D., Yi, Q., Mellad, J.A., Warren, D.T. *et al.* (2007) Nesprin-1 and -2 are involved in the pathogenesis of Emery–Dreifuss muscular dystrophy and are critical for nuclear envelope integrity. *Hum. Mol. Genet.*, **16**, 2816–2833.
37. Sutherland, H.G., Newton, K., Brownstein, D.G., Holmes, M.C., Kress, C., Semple, C.A. and Bickmore, W.A. (2006) Disruption of Ledgf/Psip1 results in perinatal mortality and homeotic skeletal transformations. *Mol. Cell. Biol.*, **26**, 7201–7210.
38. Huang, T.S., Myklebust, L.M., Kjarlan, E., Gjertsen, B.T., Pendino, F., Bruserud, O., Doskeland, S.O. and Lillehaug, J.R. (2007) LEDGF/p75 has increased expression in blasts from chemotherapy-resistant human acute myelogenic leukemia patients and protects leukemia cells from apoptosis in vitro. *Mol. Cancer*, **6**, 31.
39. Tominaga, K., Kirtane, B., Jackson, J.G., Ikeno, Y., Ikeda, T., Hawks, C., Smith, J.R., Matzuk, M.M. and Pereira-Smith, O.M. (2005) MRG15 regulates embryonic development and cell proliferation. *Mol. Cell. Biol.*, **25**, 2924–2937.
40. Latimer, K.S., Kircher, I.M., Lindl, P.A., Dawe, D.L. and Brown, J. (1989) Leukocyte function in Pelger-Huet anomaly of dogs. *J. Leukoc. Biol.*, **45**, 301–310.
41. Lekstrom-Himes, J. and Xanthopoulos, K.G. (1998) Biological role of the CCAAT/enhancer-binding protein family of transcription factors. *J. Biol. Chem.*, **273**, 28545–28548.
42. Iwama, A., Zhang, P., Darlington, G.J., McKercher, S.R., Maki, R. and Tenen, D.G. (1998) Use of RDA analysis of knockout mice to identify myeloid genes regulated in vivo by PU.1 and C/EBPalpha. *Nucleic Acids Res.*, **26**, 3034–3043.
43. Borregaard, N., Theilgaard-Monch, K., Sorensen, O.E. and Cowland, J.B. (2001) Regulation of human neutrophil granule protein expression. *Curr. Opin. Hematol.*, **8**, 23–27.
44. Olins, A.L. and Olins, D.E. (2004) Cytoskeletal influences on nuclear shape in granulocytic HL-60 cells. *BMC Cell Biol.*, **5**, 30.
45. Brinkmann, V. and Zychlinsky, A. (2007) Beneficial suicide: why neutrophils die to make NETs. *Nat. Rev. Microbiol.*, **5**, 577–582.
46. Stewart, C.L. (1993) Production of chimeras between embryonic stem cells and embryos. *Methods Enzymol.*, **225**, 823–855.
47. Escalante-Alcalde, D., Hernandez, L., Le Stunff, H., Maeda, R., Lee, H.S., Jr, Gang, C., Sciorra, V.A., Daar, I., Spiegel, S., Morris, A.J. *et al.* (2003) The lipid phosphatase LPP3 regulates extra-embryonic vasculogenesis and axis patterning. *Development*, **130**, 4623–4637.
48. Wassif, C.A., Zhu, P., Krantz, L., Krakowiak, P.A., Battaile, K.P., Weight, C.A., Grinberg, A., Steiner, R.D., Nwokiri, N.A. and Kelley, R.I. (2001) Biochemical, phenotypic and neurophysiological characterization of a genetic mouse model of RSH/Smith–Lemli–Opitz syndrome. *Hum. Mol. Genet.*, **12**, 1631–1641.
49. Hogan, B., Beddington, R., Costantini, F. and Lacy, E. (1994) *Manipulating the Mouse Embryo: A Laboratory Manual*. Cold Spring Harbor Laboratory Press, Cold Spring Harbor, NY.
50. Cohen, T.V., Kosti, O. and Stewart, C.L. (2007) The nuclear envelope protein MAN1 regulates TGFbeta signaling and vasculogenesis in the embryonic yolk sac. *Development*, **134**, 1385–1395.
51. Pfaffl, M.W. (2001) A new mathematical model for relative quantification in real-time RT-PCR. *Nucleic Acids Res.*, **29**, e45.
52. Miller, M., Shuman, J.D., Sebastian, T., Dauter, Z. and Johnson, P.F. (2003) Structural basis for DNA recognition by the basic region leucine zipper transcription factor CCAAT/enhancer-binding protein alpha. *J. Biol. Chem.*, **278**, 15178–15184.
53. Kim, J., Cantwell, C.A., Johnson, P.F., Pfarr, C.M. and Williams, S.C. (2002) Transcriptional activity of CCAAT/enhancer-binding proteins is controlled by a conserved inhibitory domain that is a target for sumoylation. *J. Biol. Chem.*, **277**, 38037–38044.
54. Kaplow, L.S. (1965) Simplified myeloperoxidase stain using benzidine dihydrochloride. *Blood*, **26**, 215–219.
55. Kuhns, D.B. (2001) In Rich, R.T.F., Kotzin, B.L. and Schroeder, H.W. (eds), *Clinical Immunology*. Harcourt International, London, pp. 121–123.
56. Johnson, P.F. (1993) Identification of C/EBP basic region residues involved in DNA sequence recognition and half-site spacing preference. *Mol. Cell. Biol.*, **13**, 6919–6930.